**Smart Structures Systems**, *Vol. 19, No. 4 (2017) 403-413*
DOI: https://doi.org/10.12989/sss.2017.19.4.403


# Optimal vibration energy harvesting from nonprismatic piezolaminated beam

Alok R Biswal[a], Tarapada Roy[*] and Rabindra K Behera[b]

*Department of Mechanical Engineering, National Institute of Technology Rourkela, Rourkela-769008, Odisha, India*

*(Received June 19, 2016, Revised October 4, 2016, Accepted December 11, 2016)*

**Abstract.** The present article encompasses a nonlinear finite element (FE) and genetic algorithm (GA) based optimal vibration energy harvesting from nonprismatic piezo-laminated cantilever beams. Three cases of cross section profiles (such as linear, parabolic and cubic) are modelled to analyse the geometric nonlinear effects on the output responses such as displacement, voltage, and power. The simultaneous effects of taper ratios (such as breadth and height taper) on the output power are also studied. The FE based nonlinear dynamic equation of motion has been solved by an implicit integration method (i.e., Newmark method in conjunction with the Newton-Raphson method). Besides this, a real coded GA based constrained optimization scheme has also been proposed to determine the best set of design variables for optimal harvesting of power within the safe limits of beam stress and PZT breakdown voltage.

**Keywords:** geometric nonlinearity; piezoelectricity; nonprismatic beam; finite element; genetic algorithm; optimal energy harvesting

## 1. Introduction

The process of extracting waste energy and converting it as usable electric energy is termed as energy harvesting or scavenging. In recent years, energy harvesting put a remarkable milestone in the field of micro electrical, mechanical system (MEMS) technology along with wireless technology due to a shortage of power consumption. In fact, energy harvesting is treated as the premium alternative sources of power for a longer period comparing to the conventional battery. Among several energy harvesting methodologies, piezoelectric is treated as the best alternative because of its ease of application and ability to cover a wide range of frequencies. In comparison to several piezoelectric energy harvesting structures, the cantilever type is best suitable due to its low resonance frequency and high average strain. However, the use of nonprismatic beams shows an effective improvement of output power due to uniform strain profiles compared to prismatic beams. These nonprismatic beams are not only selected to optimize the strength to weight ratio of the structure but also to meet the architectural and aesthetical needs. In addition to this, the geometric nonlinear effects due to large deformation of such structures cannot be overlooked. With the inclusion of geometric nonlinear effects, an accurate estimation of the voltage sensed by piezoelectric materials along with output power can be determined.

Further, the output power from the nonprismatic beam is greatly influenced by many design variables such as breadth taper, height taper, and thickness of PZT patch respectively. It is also perceived from the literature study, that the external resistance has a significant influence on the output power due to the presence of an electric circuit. These design variables may have different values to obtain output power which may cause the bending failure of the beam as well as PZT using the conventional trial and error method. Hence difficulty arises in getting the best possible set of design variables for maximizing the output power from the proposed beam. In this circumstance, optimization technique has a significant role to select the best possible design variables so as to operate the proposed beam within the safe design. Among several optimization techniques, GA is chosen because it is adaptive heuristic search algorithm based on natural selection and it doesn't require any auxiliary knowledge or derivatives of information. Moreover, unlike binary coded GA, real coded GA is more effective as design variables work directly instead of coding and decoding with less computational complexity. Based on the above scenario, the present work emphasized on the analysis of the proposed beam by selecting the best set of design variables to avoid the premature failure of the beam.

Although several works related to piezoelectric energy harvesting are carried out, some of the recent works in this direction are discussed herewith. The piezoelectric based energy harvesting, with different mechanical structures to transfer the vibration energy into piezoelectric material were discussed by Mukherjee and Chaudhuri (2005), Roundy *et al*. (2005), Hong *et al*. (2006) and Xue *et al*. (2008). Among the mechanical structures, cantilever beam has put remarkable footstep because of its low resonant frequency and high average strain. However, less possibility of extracting the maximum amount of energy from the existing cantilever based energy harvesters. Therefore more

∗Corresponding author, Assistant Professor
E-mail: tarapada@nitrkl.ac.in
[a]Ph.D. Student
E-mail: alokbiswal82@gmail.com
[b]Associate Professor
E-mail: rabi57@rediffmail.com



ISSN: 1738-1584 (Print), 1738-1991 (Online)

emphasis has been given towards the design of the beam so as to extract maximum output power. Some of the works were carried out to improve the harvested power using linear tapered cantilever beams by Benasciutti *et al*. (2010), Dietl and Garcia (2010) and Mehraeen *et al*. (2010). The energy harvesting from a bluff body subjected to transverse galloping oscillations with different cross-section geometries (such as square, D, and triangular) were investigated by Abdelkefi *et al*. (2013). The effect of shape variations (such as linear and quadratic) of a cantilever beam on the performance of energy harvester was examined by Ayed *et al*. (2013). Rosa and De Marqui Junior (2014) modelled an electromechanically coupled beam with varying cross-sectional area (trapezoidal taper and reversed trapezoidal taper) for energy harvesting. Biswal *et al*. (2015) established a finite element and genetic algorithm based vibration energy harvesting from a tapered piezolaminated cantilever beam. In their work, the effects of tapers (both in the width and height directions) on output power for three cases of shape profiles (such as linear, parabolic and cubic) were analysed.

Some of the research work related to energy harvesting with geometric nonlinear effects based on classical solutions are focussed herewith. A multi layered cantilever energy harvester having a tip mass with geometric, inertia and piezoelectric nonlinearities was studied by Abdelkefi *et al*. (2012). The piezoelectric energy harvester subjected to both base excitation and vortex-induced vibration considering both linear and nonlinear analyses was investigated by Dai *et al*. (2014). An aero-electromechanical model, in which nonlinear responses under the combined effect of galloping and base excitations was studied by Bibo *et al*. (2015). An enhanced broadband low-frequency piezo magnetoelastic energy harvester with nonlinear distributed parameter was examined by Abdelkefi and Barsallo (2016). Further, an elaborate study was carried out for energy harvesting from various nonlinear aeroelastic vibration mechanisms by Abdelkefi (2016). The effects of structural and aerodynamic nonlinearities on the performance of the harvester were deliberated by Javed *et al*. (2016). The behaviour of aeroelastic energy harvesters using the Hopf bifurcation was investigated by Bichiou *et al*. (2016).

The works related to the direction real coded GA based optimization techniques are presented herewith. A GA based linear quadratic regulator (LQR) scheme for optimal vibration control of smart fiber reinforced composite structure was established by Roy and Chakraborty (2008). Later, an improved GA based LQR control scheme for vibration control of smart fiber reinforced polymer (FRP) composite shell structures under combined mechanical and thermal loading also was presented by Roy and Chakraborty (2009a). Further, an improved real coded GA was established, which was based on optimal vibration control of composite shell structures by Roy and Chakraborty (2009b). The binary and real-coded genetic algorithms were parallelized using '*C*' and the bottlenecks of the analysis were identified and modified appropriately by Arora *et al*. (2010). A simple and efficient real-coded GA for constrained real-parameter optimization were projected by Chuang *et al*. (2016).

Even though several research works have been carried out for energy harvesting from piezolaminated beams, still some unfilled gaps in the direction of modelling and analysis of arbitrarily varying cross section profiles need to be highlighted. Moreover, FE based geometric nonlinear effects on the output power along with optimised design variables have yet to be discussed. In pertaining to these, the present work deals with a comparative study of cross section profiles of the modelled beams (such as linear, parabolic and cubic shape variations) with geometric nonlinear effects to analyse the responses such as output voltage and power. The present work also lay an emphasis on the determination of a best set of design variables for maximizing the output power incorporating a real coded GA based constrained (such as ultimate stress and breakdown voltage) optimization technique to avoid the underestimation and over estimation of power, and premature failure of the beam.

## 2. Mathematical formulation for vibrational energy harvesting

The mathematical formulations involve the modelling of three cross section profiles (such as linear, parabolic and cubic profiles) and an electric interface to obtain the output power with geometric nonlinear effects. Further, as the proposed model has several design variables which vary arbitrarily to obtain the maximum output power; it is difficult to get the best set of design variables satisfying the same. Therefore, a real coded GA based constrained optimization technique is developed to get the best set of design variables within the range of maximum output power to avoid the premature failure of the beam. The details of the formulations are articulated in the following subsections.

### *2.1 Mathematical modeling of cross sections of the beam*

Three different cross section profiles (such as linear, parabolic and cubic shape variations) are modelled for energy harvesting as

$$\text{Case (A)} \qquad A(x) = A_0\left(1 - c_b \frac{x}{L_b}\right)\left(1 - c_h \frac{x}{L_b}\right) \tag{1}$$

$$\text{Case (B)} \qquad A(x) = A_0\left(1 - c_b \frac{x}{L_b}\right)^2\left(1 - c_h \frac{x}{L_b}\right)^2 \tag{2}$$

$$\text{Case (C)} \qquad A(x) = A_0\left(1 - c_b \frac{x}{L_b}\right)^3\left(1 - c_h \frac{x}{L_b}\right)^3 \tag{3}$$

The geometric profiles of the modelled beams are shown in Figs. 1(a)-(c). The length of the beam is represented as $L_b$. The breadth and height taper ratios of the beam are denoted

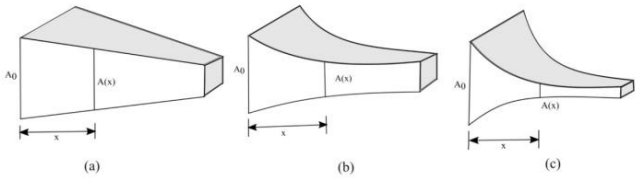


Fig. 1 Geometric profiles of (a) Linear profile (b) Parabolic profile(c) Cubic profile

as $c_b$ and $c_h$, which could vary in the range of $0 \le c_b \le 1$ and $0 \le c_h \le 1$ respectively. When $c_b=c_h=0$, the beam will become a uniform one and when $c_b=c_h=1$ the beam would taper to a point at $x=L_b$, which is a theoretical limit and is not practical. The transverse cross sectional area of the beam near the clamped end is $A_0$ which gradually decreases towards the free end as shown in Figs. 1(a)-(c).

### *2.2 Finite element modelling and analysis of piezolaminated beam*

A nonprismatic piezolaminated cantilever beam is shown in Fig. 2. The piezoelectric patch is glued on one distinct section of the surface of the beam. The stiffness and mass of the bonding agent between the PZT and host structure are neglected. The piezolaminated cantilever beam is modelled using one piezoelectric patch, which includes sensor dynamics and the remaining beam elements as classical beam theory.

#### *2.2.1 Displacement field of the beam*

The displacement field of the beam along $x$, $y$ and $z$ direction can be written as

$$\begin{aligned} u(x,y,z,t) &= u_0 - z\varphi(x,t) = u_0 - z\left(\frac{\partial w_0}{\partial x}\right) \\ v(x,y,z,t) &= 0, \\ w(x,y,z,t) &= w_0(x,t) \end{aligned} \tag{4}$$

where $u$, $v$, $w$ are the time dependent axial, lateral and transverse displacements along $x$, $y$, $z$ axes respectively. The terms $u_0$ and $w_0$ are the axial and transverse displacement of any point in the mid plane ($z$=0). $\phi$ is the rotation of the mid plane about $y$ axis and t denotes the time respectively. Consider a beam element with three degrees of freedom per node with varying cross sectional dimensions along the element axis shown in Fig. 3, where $u_1$, $v_1$, $\theta_1$ are the axial, transverse and rotation degrees of freedom at node 1 and

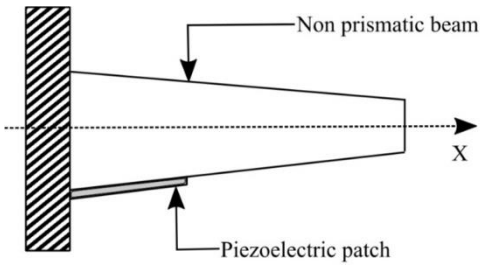


Fig. 2 Cantilever beam with piezoelectric patch

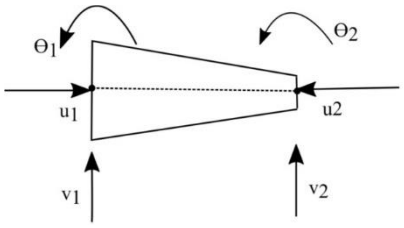


Fig. 3 Nodal degrees of freedom of nonprismatic beam element

$u_2$, $v_2$, $\theta_2$ are the corresponding degrees of freedom at node 2 respectively.

#### *2.2.2 Strain-displacement relations*

As the modelled beam length is too high as compared to the cross sectional dimensions of the beam, the shear strains are assumed to be zero. Moreover according to Von Karman hypothesis, omitting the large strain components but retaining the square of the rotation of normal transverse line in the beam, the modified strain becomes

$$\varepsilon_1 = \frac{\partial u_0}{\partial x} - z\frac{\partial^2 w_0}{\partial x^2} + \frac{1}{2}\left(\frac{\partial w_0}{\partial x}\right)^2. \tag{5}$$

The Eq. (5) can be represented in matrix form as

$$\varepsilon_1 = \begin{bmatrix} 1 & z \end{bmatrix}\{\varepsilon\} \tag{6}$$

where

$$\varepsilon = \begin{Bmatrix} \dfrac{\partial u_0}{\partial x} \\ -\dfrac{\partial^2 w_0}{\partial x^2} \end{Bmatrix} + \begin{Bmatrix} \dfrac{1}{2}\left(\dfrac{\partial w_0}{\partial x}\right)^2 \\ 0 \end{Bmatrix} \tag{7}$$

The first term of the Eq. (7) is the linear strain parameter and the second term is the geometric nonlinear strain parameters. The linear strain consists of both linear membrane strain and bending strain.

#### *2.2.3 Shape functions*

The displacement field could be interpolated in terms of degrees of freedom of nodes and shape functions based on the concept of FEM as

$$\{r\} = \begin{bmatrix} u_0(x) \\ w_0(x) \end{bmatrix} = \begin{bmatrix} N_u & 0 \\ 0 & N_w \end{bmatrix}\begin{Bmatrix} q_u \\ q_w \end{Bmatrix} = [N]\{q\} \tag{8}$$

where $N_u$ is the Lagrange and $N_w$ is the Hermite cubic interpolation or shape functions and $q$ is the elemental nodal degrees of freedoms respectively. The accuracy of the result depends on how well these shape functions are selected. These interpolation functions for a beam element can be written as

$$\begin{aligned} N_u &= \begin{bmatrix} 1-\dfrac{x}{L} & \dfrac{x}{L} \end{bmatrix} \\ N_w &= \begin{bmatrix} 1-\dfrac{3x^2}{L}+\dfrac{2x^3}{L^3} & x-\dfrac{2x^2}{L}+\dfrac{x^3}{L^2} & \dfrac{3x^2}{L^2}-\dfrac{2x^3}{L^3} & -\dfrac{x^2}{L}+\dfrac{x^3}{L^2} \end{bmatrix}. \end{aligned} \tag{9}$$

The elemental nodal displacement vector can be represented as

$$\{q_u\}=\begin{bmatrix}u_1 & u_2\end{bmatrix} \text{ and } \{q_w\}=\begin{bmatrix}v_1 & \theta_1 & v_2 & \theta_2\end{bmatrix}$$
$$\{q\}^T=\begin{bmatrix}q_u^T & q_w^T\end{bmatrix} \quad (10)$$

### 2.2.4 Coupled constitutive relationships

The constitutive relationships of the piezolaminated beam are considered for the analysis. It has been assumed that the piezoelectric continuum is exposed to both elastic and electric field. The three dimensional linear constitutive equations considering the coupling between elastic and electric fields for piezoceramic can be expressed as (Moheimani and Fleming 2006)

$$\begin{bmatrix}\varepsilon\\ D\end{bmatrix}=\begin{bmatrix}S^E & d^T\\ d & \xi^\sigma\end{bmatrix}\begin{bmatrix}\sigma\\ E\end{bmatrix} \quad (11)$$

where $\sigma$, $\varepsilon$, $E$, and $D$ are the field variable terms signifying stress components, strain components, electric field components and the electric displacement components respectively. The terms $S$, $d$, $\xi$ represents the matrix of compliance coefficients, piezoelectric strain constants, and permittivity respectively. The superscripts $E$, $\sigma$ and $T$ denote the constant electric field, stress and the transpose of the matrices respectively. The expanded form of the Eq. (11) can be written as

$$\begin{bmatrix}\varepsilon_1\\ \varepsilon_2\\ \varepsilon_3\\ \varepsilon_4\\ \varepsilon_5\\ \varepsilon_6\end{bmatrix}=\begin{bmatrix}S_{11}^E & S_{12}^E & S_{13}^E & S_{14}^E & S_{15}^E & S_{16}^E\\ S_{21}^E & S_{22}^E & S_{23}^E & S_{24}^E & S_{25}^E & S_{26}^E\\ S_{31}^E & S_{32}^E & S_{33}^E & S_{34}^E & S_{35}^E & S_{36}^E\\ S_{41}^E & S_{42}^E & S_{43}^E & S_{44}^E & S_{45}^E & S_{46}^E\\ S_{51}^E & S_{52}^E & S_{53}^E & S_{54}^E & S_{55}^E & S_{56}^E\\ S_{61}^E & S_{62}^E & S_{63}^E & S_{64}^E & S_{65}^E & S_{66}^E\end{bmatrix}\begin{bmatrix}\sigma_1\\ \sigma_2\\ \sigma_3\\ \sigma_4\\ \sigma_5\\ \sigma_6\end{bmatrix}+\begin{bmatrix}d_{11} & d_{21} & d_{31}\\ d_{12} & d_{22} & d_{32}\\ d_{13} & d_{23} & d_{33}\\ d_{14} & d_{24} & d_{34}\\ d_{15} & d_{25} & d_{35}\\ d_{16} & d_{26} & d_{36}\end{bmatrix}\begin{bmatrix}E_1\\ E_2\\ E_3\end{bmatrix} \quad (12)$$

$$\begin{bmatrix}D_1\\ D_2\\ D_3\end{bmatrix}=\begin{bmatrix}d_{11} & d_{12} & d_{13} & d_{14} & d_{15} & d_{16}\\ d_{21} & d_{22} & d_{23} & d_{24} & d_{25} & d_{26}\\ d_{31} & d_{32} & d_{33} & d_{34} & d_{35} & d_{36}\end{bmatrix}\begin{bmatrix}\sigma_1\\ \sigma_2\\ \sigma_3\\ \sigma_4\\ \sigma_5\\ \sigma_6\end{bmatrix}+\begin{bmatrix}\xi_{11}^\sigma & \xi_{12}^\sigma & \xi_{13}^\sigma\\ \xi_{21}^\sigma & \xi_{22}^\sigma & \xi_{23}^\sigma\\ \xi_{31}^\sigma & \xi_{32}^\sigma & \xi_{33}^\sigma\end{bmatrix}\begin{bmatrix}E_1\\ E_2\\ E_3\end{bmatrix} \quad (13)$$

Assuming that the piezoceramic material is poled along the axis 3 and viewing it as transversely isotropic, many parameters in the above expression are either zero or can be expressed in terms of other parameters. Subsequently, the Eqs. (12) and (13) are simplified to

$$\begin{bmatrix}\varepsilon_1\\ \varepsilon_2\\ \varepsilon_3\\ \varepsilon_4\\ \varepsilon_5\\ \varepsilon_6\end{bmatrix}=\begin{bmatrix}S_{11}^E & S_{12}^E & S_{13}^E & 0 & 0 & 0\\ S_{12}^E & S_{11}^E & S_{13}^E & 0 & 0 & 0\\ S_{13}^E & S_{13}^E & S_{33}^E & 0 & 0 & 0\\ 0 & 0 & 0 & S_{44}^E & 0 & 0\\ 0 & 0 & 0 & 0 & S_{44}^E & 0\\ 0 & 0 & 0 & 0 & 0 & 2(S_{11}^E-S_{12}^E)\end{bmatrix}\begin{bmatrix}\sigma_1\\ \sigma_2\\ \sigma_3\\ \sigma_4\\ \sigma_5\\ \sigma_6\end{bmatrix}+\begin{bmatrix}0 & 0 & d_{31}\\ 0 & 0 & d_{31}\\ 0 & 0 & d_{33}\\ 0 & d_{15} & 0\\ d_{15} & 0 & 0\\ 0 & 0 & 0\end{bmatrix}\begin{bmatrix}E_1\\ E_2\\ E_3\end{bmatrix} \quad (14)$$

$$\begin{bmatrix}D_1\\ D_2\\ D_3\end{bmatrix}=\begin{bmatrix}0 & 0 & 0 & 0 & d_{15} & 0\\ 0 & 0 & 0 & d_{15} & 0 & 0\\ d_{31} & d_{31} & d_{33} & 0 & 0 & 0\end{bmatrix}\begin{bmatrix}\sigma_1\\ \sigma_2\\ \sigma_3\\ \sigma_4\\ \sigma_5\\ \sigma_6\end{bmatrix}+\begin{bmatrix}\xi_{11}^\sigma & 0 & 0\\ 0 & \xi_{11}^\sigma & 0\\ 0 & 0 & \xi_{33}^\sigma\end{bmatrix}\begin{bmatrix}E_1\\ E_2\\ E_3\end{bmatrix} \quad (15)$$

The piezoelastic behavior of the structure is modelled as a thin beam based on the Euler-Bernoulli beam theory, hence the stress components other than the one-dimensional bending stress $\sigma_1$ are negligible, so that

$$\sigma_2=\sigma_3=\sigma_4=\sigma_5=\sigma_6=0. \quad (16)$$

The Eqs. (14) and (15) can be reduced to

$$\varepsilon_1=S_{11}^E\sigma_1+d_{31}E_3 \quad (17)$$

$$D_3=d_{31}\sigma_1+\xi_{33}^\sigma E_3 \quad (18)$$

The Eqs. (17) and (18) can further be converted to

$$\sigma_1=\bar{c}_{11}^E\varepsilon_1-\bar{e}_{31}E_3 \quad (19)$$

$$D_3=\bar{e}_{31}\varepsilon_1+\bar{\xi}_{33}^\varepsilon E_3 \quad (20)$$

where the terms used are expressed as

$$\bar{c}_{11}^E=\frac{1}{S_{11}^E},\bar{e}_{31}=\frac{d_{31}}{S_{11}^E},\bar{\xi}_{33}^\varepsilon=\xi_{33}^\sigma-\frac{d_{31}^{\ 2}}{S_{11}^E} \quad (21)$$

### 2.2.5 Electric potential in the piezoelectric patch

The electric potential function $v$ is assumed to vary linearly along the thickness direction and is constant in $x$ and $y$ direction in the piezoelectric layer. The difference in electric potential at the top and the bottom surface of the piezoelectric layer is constant, and thus they form equipotential surfaces. For a thin piezoelectric patch, the electric field in the thickness direction is dominant henceforth; it can be considered as a nonzero component only in the thickness direction. With this approximation, the electric field strength in terms of the electric potential for the piezoelectric patch can be represented as

$$E_3=[B_v]\{v(t)\} \quad (22)$$

where $[B_v]$ is the electric field gradient, and $v(t)$ is the electric potential. Due to the presence of a piezoelectric patch, an additional degree of freedom is introduced at the elemental level.

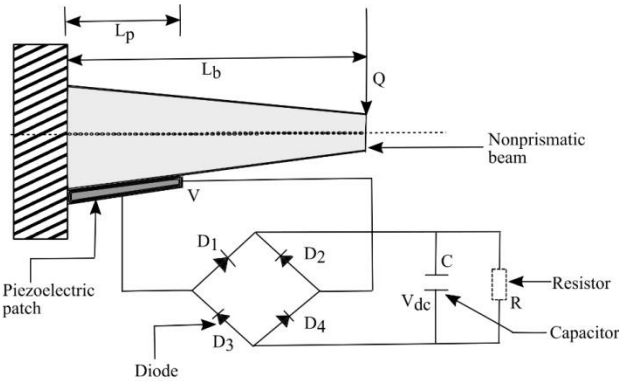


Fig. 4 Piezolaminated cantilever beam with the classic electric interface

### *2.2.6 Governing equation*

Fig. 4 shows a piezolaminated cantilever beam with PZT patch near the clamped end. An electric interface is connected to both surfaces of the piezolaminated patch for power generation. The cantilever beam is subjected to an external excitation $Q$ at its free end. Using Hamilton's principle, the dynamic equations of motion of the piezolaminated beam for energy harvesting system can be expressed as

$$\partial \Pi = \int_{t_1}^{t_2} [\partial (E_K - E_P + W)] dt = 0 \tag{23}$$

where $E_k$ denotes the kinetic energy, $E_p$ denotes the electromechanical enthalpy and $W$ denotes the work done. The terms $t_1$ and $t_2$ represents the initial and final time. The expressions for $E_k$, $E_p$, and $W$ of the piezolaminated beam can be obtained by the following expressions as

$$E_k = \frac{1}{2}\int_{V_b} \rho_b \dot{r}^T \dot{r} dV_b + \frac{1}{2}\int_{V_p} \rho_p \dot{r}^T \dot{r} dV_p \tag{24}$$

$$E_p = \frac{1}{2}\int_{V_b} \varepsilon_1^{\ T} \sigma_1 dV_b + \frac{1}{2}\int_{V_p} \varepsilon_1^{\ T} \sigma_1 dV_p - \frac{1}{2}\int_{V_p} E_3^{\ T} D_3 dV_p \tag{25}$$

$$W = \sum_{i=1}^{nf} r(x_i) Q(x_i) - \sum_{j=1}^{nq} v.\overline{G}_j \tag{26}$$

The terms $V_b$ and $V_p$, denote the volume of beam and piezoelectric patch, $n_f$ and $n_q$ denote the number of externally applied load and piezoelectric patches over which the charge developed, and $\bar{G}_j$ is the charge developed over the piezoelectric patch respectively. For open circuit condition, the differences of electrical potential between the electrodes are unknown considering charge equal to zero ($\bar{G}_j = 0$). Now using Eqs. (19), (20), (22), (24), (25), (26), the Eq. (23) can be written as

$$\partial \Pi = \int_{t_1}^{t_2} \left[ \begin{array}{l} \int_{V_b} \frac{1}{2}\rho_b \partial \dot{r}^T \dot{r} dV_b + \int_{V_p} \frac{1}{2}\rho_p \partial \dot{r}^T \dot{r} dV_p - \int_{V_b} \frac{1}{2}\partial \varepsilon_1^{\ T} \bar{c}_{11}^E \varepsilon_1 dV_b - \int_{V_p} \frac{1}{2}\partial \varepsilon_1^{\ T} \bar{c}_{11}^E \varepsilon_1 dV_p + \int_{V_p} \frac{1}{2}\partial \varepsilon_1^{\ T} \bar{e}_{31} E_3 dV_p \\ + \int_{V_p} \frac{1}{2}\partial E_3^T \bar{e}_{31} \varepsilon_1 dV_p + \int_{V_p} \frac{1}{2}\partial E_3^T \bar{\xi}_{33}^{\varepsilon} E_3 dV_p + \sum_{i=1}^{nf} \partial r(x_i) Q(x_i) \end{array} \right] \tag{27}$$

From the Eq. (27), the elemental mass matrices for both in plane and bending of the beam and the piezoelectric patch can be derived as

$$[M_{bu}] = \int_0^{L_b} [N_u]^T \rho_b A_b [N_u] dx \ , \ [M_{bw}] = \int_0^{L_b} [N_w]^T \rho_b A_b [N_w] dx. \tag{28}$$

$$[M_{pu}] = \int_0^{L_p} [N_u]^T \rho_p A_p [N_u] dx, [M_{pw}] = \int_0^{L_p} [N_w]^T \rho_p A_p [N_w] dx \ . \tag{29}$$

where $\rho$ and $A$ represents the mass density and transverse cross sectional area, the suffix $b$ and $p$ represents the beam and the piezoelectric patch respectively.The terms $M_{bu}$, $M_{pu}$, $M_{bw}$ and $M_{pw}$ are the linear element mass matrices for in plane (stretching) and out of plane (bending) displacements respectively. Similarly, the elemental stiffness matrices of the beam as well as the piezoelectric patch for in plane, bending and geometric nonlinear cases can be derived as

$$\begin{array}{l} [K_{bu}] = \int_0^{L_b} [N_{u,x}]^T E_b A_b [N_{u,x}] dx \ , \ [K_{bw}] = \int_0^{L_b} [N_{w,xx}]^T E_b I_b [N_{w,xx}] dx \ , \\ [K_{b2}] = \int_0^{L_b} \frac{1}{2}[N_{u,x}]^T E_b A_b \left(\frac{\partial w_0}{\partial x}\right) [N_{w,x}] dx \ , \ [K_{b3}] = \int_0^{L_b} [N_{u,x}] E_b A_b \left(\frac{\partial w_0}{\partial x}\right) [N_{w,x}]^T dx \text{ and} \\ [K_{b4}] = \int_0^{L_b} [N_{w,x}]^T E_b A_b \left(\frac{\partial w_0}{\partial x}\right)^2 [N_{w,x}] dx. \end{array} \tag{30}$$

$$\begin{array}{l} [K_{pu}] = \int_0^{L_p} [N_{u,x}]^T E_p A_p [N_{u,x}] dx \ , \ [K_{pw}] = \int_0^{L_p} [N_{w,xx}]^T E_p I_p [N_{w,xx}] dx \ , \\ [K_{p2}] = \int_0^{L_p} \frac{1}{2}[N_{u,x}]^T E_p A_p \left(\frac{\partial w_0}{\partial x}\right) [N_{w,x}] dx \ , \ [K_{p3}] = \int_0^{L_p} [N_{u,x}] E_p A_p \left(\frac{\partial w_0}{\partial x}\right) [N_{w,x}]^T dx \text{ and} \\ [K_{p4}] = \int_0^{L_p} [N_{w,x}]^T E_p A_p \left(\frac{\partial w_0}{\partial x}\right)^2 [N_{w,x}] dx. \end{array} \tag{31}$$

The terms $K_{bu}$, $K_{pu}$, $K_{bw}$, and $K_{pw}$, are the linear element stiffness matrices for in plane (stretching) and out of plane (bending) displacements, the terms $K_{b2}$, $K_{p2}$, $K_{b3}$, $K_{p3}$, $K_{b4}$, and $K_{p4}$ are the nonlinear elemental stiffness matrices for both beam and piezoelectric patch respectively. Similarly, the elemental electromechanical coupling matrices of beam and piezo-patch and the capacitance matrix can be obtained as

$$\begin{array}{l} [K_{bpu}] = -\int_0^{L_p} z A_p \bar{e}_{31} [B_V][N_{u,x}]^T dx \ , [K_{bpw}] = -\int_0^{L_p} z A_p \bar{e}_{31} [B_V][N_{w,xx}]^T dx \text{ and} \\ [K_{bp5}] = -\int_0^{L_p} z A_p \bar{e}_{31} [B_V] \left(\frac{\partial w_0}{\partial x}\right) [N_{w,x}]^T dx \text{ and } [K_{pp}] = \int_0^{L_p} [B_v]^T A_p \bar{\xi}_{33} [B_v] dx \ . \end{array} \tag{32}$$

Where $K_{bpu}$ and $K_{bpw}$ are the element coupling matrices for in plane (stretching) and out of plane (bending) displacements, $K_{bp5}$ is the nonlinear coupling matrix, and $K_{pp}$ is the capacitance matrix respectively. The elemental mass and stiffness of the agent used for bonding between the piezoelectric material and substrate are neglected. The stiffness, mass, and coupling matrices have been evaluated by numerical integration using two point Gauss quadrature method. After assembling the elemental matrices, the global set of equations are found. The governing equation in elemental matrix form of the piezolaminated beam can be written as

$$\begin{array}{r} \begin{bmatrix} M_{bu} & 0 \\ 0 & M_{bw} \end{bmatrix} \begin{Bmatrix} \ddot{q}_u \\ \ddot{q}_w \end{Bmatrix} + \begin{bmatrix} M_{pu} & 0 \\ 0 & M_{pw} \end{bmatrix} \begin{Bmatrix} \ddot{q}_u \\ \ddot{q}_w \end{Bmatrix} + \begin{bmatrix} K_{bu} & K_{b2} \\ K_{b3} & K_{bw} + K_{b4} \end{bmatrix} \begin{Bmatrix} q_u \\ q_w \end{Bmatrix} + \begin{bmatrix} K_{pu} & K_{p2} \\ K_{p3} & K_{pw} + K_{p4} \end{bmatrix} \begin{Bmatrix} q_u \\ q_w \end{Bmatrix} \\ - \begin{bmatrix} K_{bpu} \\ K_{bpw} + K_{bp5} \end{bmatrix} \{v(t)\} = \{Q\} \\ \begin{bmatrix} K_{bpu} \\ K_{bpw} + K_{bp5} \end{bmatrix}^T \begin{Bmatrix} q_u \\ q_w \end{Bmatrix} + [K_{pp}]\{v(t)\} = \{0\} \end{array} \tag{33}$$

The piezolaminated beam is modeled in two domains i.e. mechanical and electrical domain. In a mechanical domain, the beam is clamped at one end, and the other end is free. In electrical domain the piezoelectric element is open-circuited; the differences of electric potentials between their electrodes are unknown and can be evaluated using the second line of Eq. (33), such that

$$v(t) = -[K_{pp}]^{-1} \begin{bmatrix} K_{bpu} \\ K_{bpw} + K_{bp5} \end{bmatrix}^T \begin{Bmatrix} q_u \\ q_w \end{Bmatrix} \tag{34}$$

Replacing Eq. (34) in the first line of Eq. (33) leads to the condensed equation of motion

$$\left[\begin{bmatrix} M_{bu} & 0 \\ 0 & M_{bw} \end{bmatrix}+\begin{bmatrix} M_{pu} & 0 \\ 0 & M_{pw} \end{bmatrix}\right]\begin{Bmatrix} \ddot{q}_u \\ \ddot{q}_w \end{Bmatrix} + \left[\begin{bmatrix} K_{bu} & K_{b2} \\ K_{b3} & K_{bw}+K_{b4} \end{bmatrix}+\begin{bmatrix} K_{pu} & K_{p2} \\ K_{p3} & K_{pw}+K_{p4} \end{bmatrix}+\begin{bmatrix} K_{bpu} \\ K_{bpw}+K_{bp5} \end{bmatrix}\left[K_{pp}\right]^{-1}\begin{bmatrix} K_{bpu} \\ K_{bpw}+K_{bp5} \end{bmatrix}^T\right]\begin{Bmatrix} q_u \\ q_w \end{Bmatrix}=\{Q\} \tag{35}$$

From the Eq. (35), the generalised displacement can be evaluated. The electric potential generated across the electrodes can be found using Eq. (34).

### 2.2.7 Determination of output power

To incorporate the energy dissipation term into the equation, Ohm's law is used, and a resistive element is added between the top and bottom surface of the piezoelectric patch shown in Fig. 4. By incorporating the resistive element, the electrical boundary condition becomes

$$v(t) = -RI(t) \tag{36}$$

where $I(t)$ is the current output of the piezoelectric element and $R$ is the external load resistance. Now putting the Eq. (36) into Eq. (34), one can get

$$RI(t) = \left[K_{pp}\right]^{-1}\begin{bmatrix} K_{bpu} \\ K_{bpw}+K_{bp5} \end{bmatrix}^T\begin{Bmatrix} q_u \\ q_w \end{Bmatrix} \tag{37}$$

The output current of the piezoelectric element can be obtained using Eq. (37) which can be directly related to the power output through the external load resistance. Again for sensing purpose, the total charge on the electrode surface of the piezoelectric patch can be expressed as

$$Q_r = \int_A D_3 dA = \int_A \left(\bar{e}_{31}\varepsilon_1 + \bar{\xi}_{33}^{\varepsilon} E_3\right) dA \tag{38}$$

The current which is proportional to the charge on the electrode surface flowing out to the external resistance can be obtained as

$$I = \omega Q_r \tag{39}$$

where $\omega$ is the fundamental frequency of the piezolaminated beam. The Eq. (39) is valid for harmonic excitation only. From the values of current and external resistance the output power can be obtained as

$$P_{out} = I^2 R \tag{40}$$

### 2.2.8 Nonlinear system of equations

The non-linear Eq. (35) in time domain can be solved using Newmark method in conjunction with an iteration method i.e., Newton-Raphson method. By using such methods, the nonlinear differential equations of motion can be reduced to a set of non-linear algebraic equations (Reddy 2014). The nonlinear equation of motion can be written after globalising the Eq. (35) which is in the form of

$$\left[K_{eff}\right]^{t+\Delta t}\{q\} = Q_{eff}^{t+\Delta t} \tag{41}$$

where $[K_{eff}]$ and $[Q_{eff}]$ are the effective global stiffness matrix consisting of nonlinear terms and effective global load vector respectively which can be represented as

$$K_{eff} = \left[\begin{bmatrix} \bar{K}_{bu} & \bar{K}_{b2} \\ \bar{K}_{b3} & \bar{K}_{bw}+\bar{K}_{b4} \end{bmatrix}+\begin{bmatrix} \bar{K}_{pu} & \bar{K}_{p2} \\ \bar{K}_{p3} & \bar{K}_{pw}+\bar{K}_{p4} \end{bmatrix}+\begin{bmatrix} \bar{K}_{bpu} \\ \bar{K}_{bpw}+\bar{K}_{bp5} \end{bmatrix}K_{pp}^{-1}\begin{bmatrix} \bar{K}_{bpu} \\ \bar{K}_{bpw}+\bar{K}_{bp5} \end{bmatrix}^T\right] + a_0\left[\begin{bmatrix} \bar{M}_{bu} & 0 \\ 0 & \bar{M}_{bw} \end{bmatrix}+\begin{bmatrix} \bar{M}_{pu} & 0 \\ 0 & \bar{M}_{pw} \end{bmatrix}\right] \tag{42}$$

$$Q_{eff}^{t+\Delta t} = \bar{Q}^{t+\Delta t} + \left[\begin{bmatrix} \bar{M}_{bu} & 0 \\ 0 & \bar{M}_{bw} \end{bmatrix}+\begin{bmatrix} \bar{M}_{pu} & 0 \\ 0 & \bar{M}_{pw} \end{bmatrix}\right]\left\{a_0\{q\}^t + a_1\{\dot{q}\}^t + a_2\{\ddot{q}\}^t\right\}$$

The terms $\bar{K}$ and $\bar{M}$ are the global stiffness and mass matrices of the modelled beam, respectively. The terms $a_0$, $a_1$, $a_2$ given by Bathe (2006) as

$$a_0 = \frac{1}{\alpha \Delta t^2};\ a_1 = \frac{1}{\alpha \Delta t};\ a_2 = \frac{1}{2\alpha} - 1;\quad \alpha = 0.25 \tag{43}$$

Since the effective stiffness matrix is nonlinear, an iterative solution procedure i.e., Newton Raphson method has been adopted for any fixed time having $s^{th}$ iteration. In Newton Raphson method, the linearized element equation is of the form

$$\{q\}^s = \{q\}^{s-1} - \left[\left[T^{s-1}\right]^{-1}\left\{R^{s-1}\right\}\right] \tag{44}$$

where $R$ and $T$ denote the residual and the tangent stiffness matrix and can be derived as

$$\left\{R^{(s-1)}\right\} = \left[K_{eff}^{(s-1)}\right]\{q\}^{(s-1)} - Q_{eff} \quad and$$
$$\left\{T^{s-1}\right\} = \frac{\partial\left\{R^{(s-1)}\right\}}{\partial\{q\}^{(s-1)}} \tag{45}$$

In Newton- Raphson method, the first iteration can be calculated using Eq. (44) considering linear stiffness matrix assuming $\{q\}^{s-1} = 0$. The residual is calculated in each iteration and the process repeated until the residual becomes zero.

### 2.3 Electric interface

Fig. 4 represents the piezoelectric energy harvesting circuit. The interface consists of a rectifier made up of diodes, an external load resistor, and a capacitor. The diodes $D_1$, $D_2$, $D_3$, and $D_4$ are connected in the circuit along with the capacitor $C$ and resistor $R$. The voltage in the piezoelectric element and capacitor are $V$ and $V_{dc}$ respectively. When the absolute value of voltage in the piezoelectric element is lower than the voltage across the capacitor, the rectifier is in a blocked state, and the piezoelectric element is in an open circuit state. A current $I$ flows through the diodes when the absolute value of voltage in the piezoelectric element is more than the voltage across the capacitor. The current divided into two parts, one to the capacitor and the other to the load, after passing through the rectifier. Due to the current flow through the external resistor, power is generated.

### 2.4 Formulation for present optimization problem

From the present problem formulation, it is observed that the output power is mostly a function of certain design variables such as breadth taper ($c_b$), height taper ($c_h$), the thickness of PZT patch ($t_p$) and external load resistance ($R$) respectively. These design variables have different values, and consequently, it is difficult to get the best set of variables to maximize the output power. To get the best combination of the above variables, a search algorithm is required within the safe design of beam and PZT patch, respectively. Hence the objective function of the present formulation is derived as

$$P_{\max} = \left[\frac{z_1\varphi}{2\left(1+\frac{z_2 R}{t_p}\right)}\right]^2 R \quad (46)$$

$$subjected\,to\ (\sigma_{induced})_{beam} < (\sigma_{allowable})_{beam}, (\sigma_{induced})_{PZT} < (\sigma_{allowable})_{PZT}$$
$$(V_{induced})_{PZT} < (V_{allowable})_{PZT}.$$

Where the terms are denoted as $z_1 = b \times h \times \omega \times \bar{e}_{31}$ and $z_2 = b \times l_p \times \omega \times \bar{\xi}_{33}$, respectively. $\sigma_{\text{induced}}$ and $V_{\text{induced}}$ are the stress and open circuit voltage of the PZT material. The allowable stress of beam and PZT material are 550 MPa and 14 MPa, respectively specified by Flynn and Sanders (2002). The allowable voltage of piezo-ceramic material is around 500-1000 V per 1 mm piezo thickness stated by Bruch Jr *et al*. (2000).

### *2.4.1 Real coded GA for optimal power*

A real coded GA has been implemented in the present formulation to obtain the best set of parameters to maximize the output power. The flowchart of the basic genetic procedure has been shown in Fig. 5. For this analysis, four parameters are chosen for the optimization process such as breadth taper ($c_b$), height taper ($c_h$), the thickness of PZT patch ($t_p$) and external load resistance ($R$) respectively. The population size has been taken as one

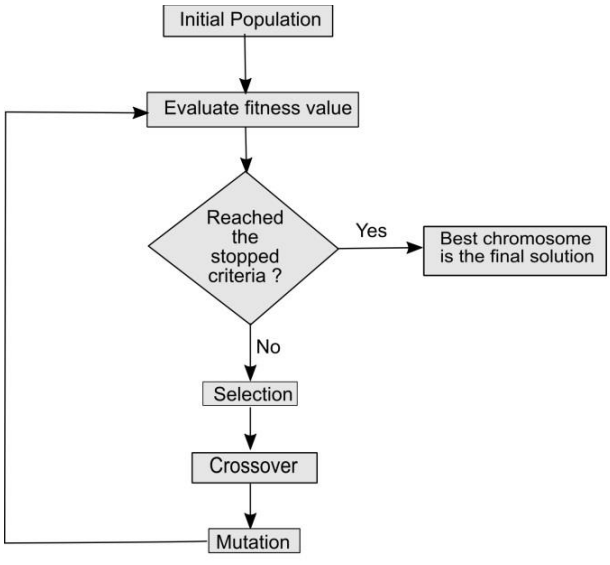


Fig. 5 Flowchart of the genetic algorithm used for the parameters optimization

hundred. The fitness function for this problem is derived as

$$H(u) = \begin{cases} P(u) & if\ (\sigma_{\text{induced}})_{beam} < (\sigma_{allowable})_{beam}\ ;\ (\sigma_{induced})_{PZT} < (\sigma_{allowable})_{PZT}\ ; \\ & \&\ (V_{induced})_{PZT} < (V_{allowable})_{PZT} \\ P(u)\alpha & otherwise \end{cases} \quad (47)$$

where $H$ is the fitness function, $u$ is the optimization parameters vector and $P$ is the power harvested respectively. $\alpha$ denotes the penalty for this algorithm which is taken as $10^{-8}$ and which used in case of constrained violation. The ranges of $c_b$, $c_h$, $t_p$ and $R$, have been taken as $0 \le c_b \le 0.8$, $0 \le c_h \le 0.8$, $0.0001 \le t_p \le 0.0004$ (Ayed *et al*. 2013) and $0 \le R \le 100000$. The algorithm is sustained for some generations until the fitness reached the optimum value and there is also no change in fitness for a large number of generations. In the present work, the real coded genetic algorithm consists of the Roulette wheel selection, simulated binary crossover (SBX) and parameter based mutation operators.

## 3. Result and discussion

Various analyses have been performed for optimal vibration energy harvesting after validating the present formulation. The validated results are presented in the following subsections.

### *3.1 Electromechanical validation*

For electromechanical validation, the obtained results are compared with already published results by Hwang and Park (1993). For this purpose, a bimorph cantilever beam is considered which is made up of two PVDF layers. The bimorph beam is subjected to an external voltage. Bending moment is caused due to the induced internal stresses which power the bimorph beam to bend. The dimensions of the beam are taken as (100×5×1) mm. The bimorph beam has been discretized into five equal finite elements. The found results with the percentage of deviation from existing results are presented in Table 1.

### *3.2 Validation of static and dynamic sensing of piezoelectric bimorph*

Further, the large deformation effect in the bimorph cantilever beam due to transverse load at its tip is investigated. The deflection ratios ($\Delta/L_b$) for different

Table 1 Transverse deflection of piezoelectric bimorph actuator

| Distance(mm)from fixed end | Deflection(μm) Hwang and Park (1993) | Deflection(μm) present code | % of deviation |
|---|---|---|---|
| 20 | 0.0131 | 0.0139 | 5.75 |
| 40 | 0.0545 | 0.0554 | 1.62 |
| 60 | 0.1200 | 0.1247 | 3.76 |
| 80 | 0.2180 | 0.2218 | 1.71 |
| 100 | 0.3400 | 0.3465 | 1.87 |

Table 2 Comparison of results for piezo bimorph cantilever beam

| $QL^2/EI$ | $(\Delta/L)_{linear}$ Mukherjee and Chaudhuri (2002) | $(\Delta/L)_{linear}$ (present) | % of deviation | $(\Delta/L)_{nonlinear}$ Mukherjee and Chaudhuri (2002) | $(\Delta/L)_{nonlinear}$ (present) | % of deviation |
|---|---|---|---|---|---|---|
| 1.11 | 0.37 | 0.36 | 2.70 | 0.35 | 0.337 | 3.71 |
| 5.55 | 1.85 | 1.84 | 0.54 | 0.75 | 0.69 | 8 |
| 13.88 | 4.63 | 4.6 | 0.64 | 0.87 | 0.88 | 1.14 |
| 16.66 | 5.55 | 5.52 | 0.54 | 0.88 | 0.93 | 5.37 |
| 27.77 | 9.25 | 9.2 | 0.54 | 0.91 | 1.01 | 9.9 |

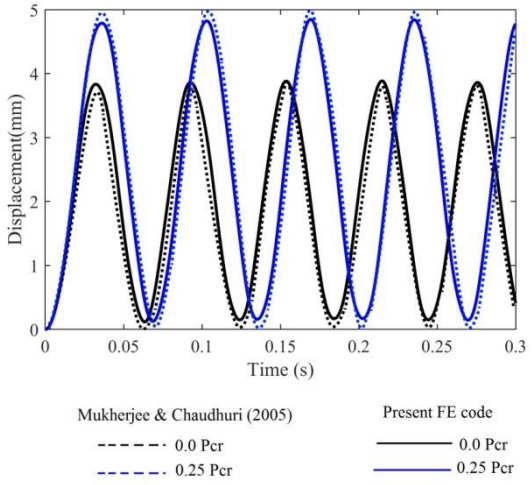


Fig. 6 Nonlinear dynamic response of piezoelectric bimorph

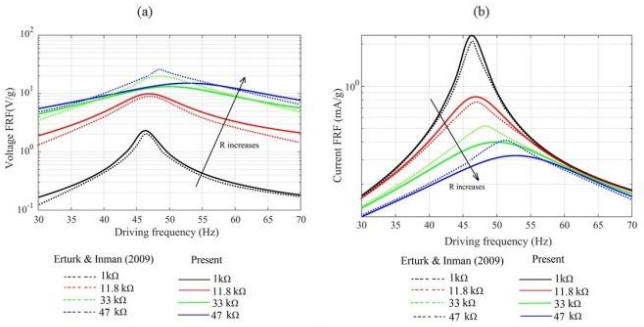


Fig. 7 Comparison of (a) voltage FRF (b) current FRF with experimental measurements

values of load ratios ($QL_b^2/EI$) are listed in Table 2. The results are corroborated by the available existing results by Mukherjee and Chaudhuri (2002).

Further, the nonlinear dynamic effect on PVDF bimorph beam has been inspected. For this purpose, one tip ramp loading of 0.005N is applied along with an axial compressive load (Mukherjee and Chaudhuri 2005).

From the Fig. 6 it has been observed that the results obtained for nonlinear response of the tip displacement of the bimorph cantilever beam for the axial loads $0.0P_{cr}$ and $0.25P_{cr}$ ($P_{cr}$ is the 1st Euler buckling load) also gives close agreement with the already published results (Mukherjee and Chaudhuri 2005)

### 3.3 Experimental validation of the present formulation

The present developed FE code has also been compared with the available experimental results (Erturk and Inman 2009) for a rectangular cantilever bimorph energy harvester with a tip mass under base excitation. The Figs. 7(a) and 7(b) show the compared results of the voltage frequency response function (FRF) and current FRF, and it has been observed that the present results are in close agreement with the already published experimental results by Erturk and Inman (2009).

### 3.4 Variation of Output power with load resistance

Figs. 8(a)-(d) show the variation of output power with external load resistance of Cases (A), (B) and (C) for $c_b$=0.2, 0.3 and $c_h$=0.2, 0.3 respectively. From the Figs. 8(a)-(b) , it is observed that the output power of Case (C) is 0.164 mW, correspondingly the values are 0.110 mW in Case (B) and 0.068 mW in Case (A) for taper values of $c_b$=0.2 and $c_h$=0.2. The optimum resistance of Case (C) has been found as 145.322 kΩ whereas, in Case (B) and (A) the values are found as 120.352 kΩ and 105.067 kΩ respectively. When the height taper changed to 0.3 the output power obtained as 0.232 mW with the optimum resistance of 197.783 kΩ in Case (C) whereas in Case (B) and Case (A) the output power obtained is 0.152 mW, 146.824 kΩ and 0.083 mW, 112.716 kΩ respectively. It indicates with an increase in height taper the output power has been increased near about 43% in Case (C) whereas in Case (B) and (A), the values are 37% and 24% respectively. Similarly, there has been an increase in optimum resistance when the height taper changed from 0.2 to 0.3. Again from Figs. 8(c) and 8(d), it has been observed that for taper

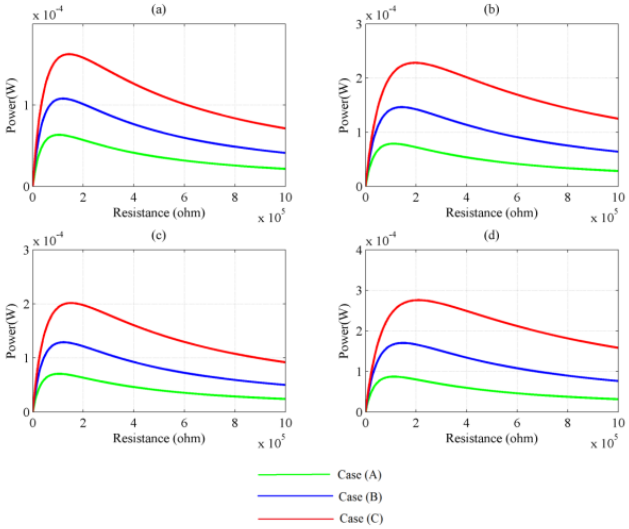


Fig. 8 Variation of output power with external load resistance of Case (A), (B) and (C) for (a) $c_b$ = 0.2, $c_h$ = 0.2, (b) $c_b$= 0.2, $c_h$ = 0.3, (c) $c_b$ = 0.3, $c_h$ = 0.2 and (d) $c_b$ = 0.3, $c_h$ = 0.3

values of $c_b$=0.3 and $c_h$=0.2 the output power along with optimum resistance of Case (C) is 0.208 mW, 154.01 kΩ whereas in Case (B) and (A) the values are 0.132 mW, 127.025 kΩ, and 0.075 mW, 108.534 kΩ respectively. As the height taper changed to 0.3 the output power has been increased to 0.285 mW in Case (C) whereas in Case (B) and Case (A) the values are 0.178 mW and 0.093 mW, correspondingly the optimum resistances in Case (C), (B) and (A) are 211.845 kΩ, 149.515 kΩ, and 115.472 kΩ respectively.

From this, it has been perceived that maximum output power obtained for an optimum resistance. Again it has been illustrated that increase in height taper more than 18% of power can be scavenged than the increase in breadth taper.

### *3.5 Nonlinear tip displacement responses*

The tip responses of the piezolaminated cantilever beam for the modeled beams have been compared and shown in Figs. 9 (a)-(d). The responses have been found for $c_b$ = 0.2, 0.3 and $c_h$= 0.2, 0.3. The peak amplitude has been calculated for all cases considering the effects of geometric nonlinearity. From the Figs. 9(a)-(d) it has been perceived that the period of vibration of Case (C) is more than Case (B) and Case (A) for different taper values. The peak amplitude of prismatic beam has been found as 0.0694 mm. From Figs. 9(a) and 9(b) it has been observed that the peak amplitude of Case (C) is 0.158 mm whereas in Case (A) and Case (B) the magnitudes are 0.095 mm and 0.128 mm, for taper values of $c_b$ = 0.2 and $c_h$ = 0.2 respectively. When the height taper changed to 0.3, the peak amplitude of Case (C) has been shifted to 0.178 mm, whereas in Case (B) and Case (A) the values are obtained as 0.139 mm and 0.0982 mm respectively. Similarly from Figs. 9(c) and 9(d), the peak amplitude of Case (C) has been found 0.1910 mm, whereas for Case (B) and (A) the values are 0.147 mm and 0.108 mm for $c_b$ = 0.3 and $c_h$ = 0.2 respectively. When the height taper increased to 0.3, the peak amplitude of case (C), (B) and (A) have been shifted to 0.2104 mm, 0.162 mm and 0.1098 mm respectively. From this, the peak amplitudes obtained showing higher values in Case (C) than Case (B) and (A).

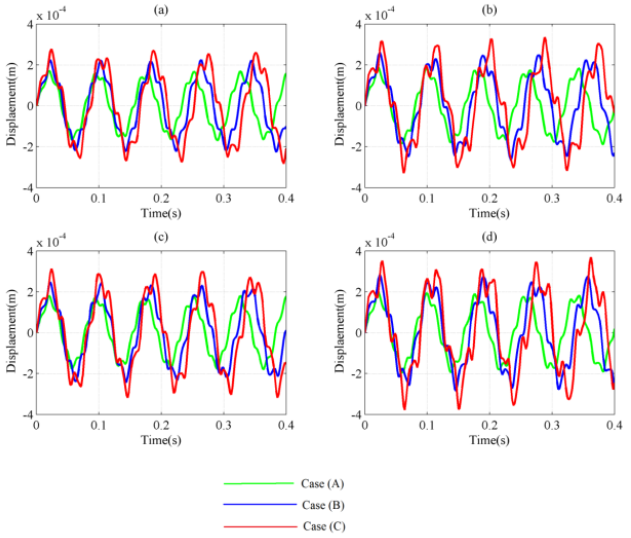


Fig. 9 Nonlinear tip displacement responses of Case (A), (B) and (C) for (a) $c_b$ = 0.2, $c_h$ = 0.2 (b) $c_b$= 0.2, $c_h$ = 0.3 (c) $c_b$ = 0.3, $c_h$ = 0.2 (d) $c_b$ = 0.3, $c_h$ = 0.3

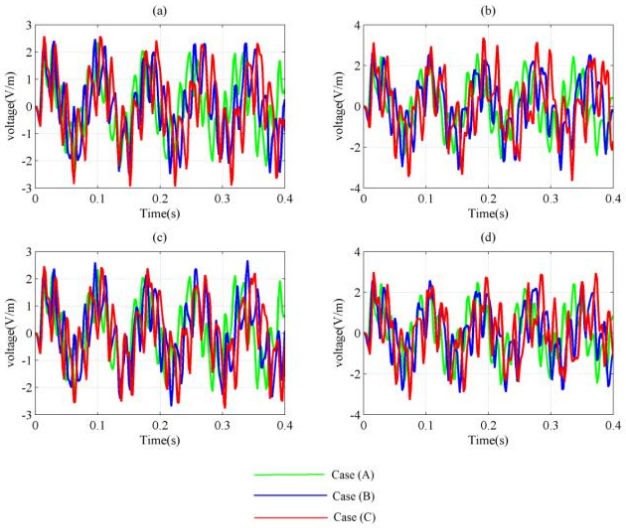


Fig. 10 Nonlinear voltage response of Case (A), (B) and (C) for (a) $c_b$ = 0.2, $c_h$ = 0.2 (b) $c_b$= 0.2, $c_h$ = 0.3 (c) $c_b$ = 0.3, $c_h$ = 0.2 (d) $c_b$ = 0.3, $c_h$ = 0.3

### *3.6 Nonlinear voltage responses*

The voltage response from the piezolaminated cantilever beam has been shown in Figs.10 (a)-(d) for $c_b$ =0.2, 0.3 and $c_h$ = 0.2, 0.3 respectively. It has been observed that the peak voltage of Case (C) increased to 86% for $c_b$ = 0.3 and $c_h$ = 0.3, whereas an increase in 50% in Case (B) and 32% in Case (A) compared to prismatic beams. From this, it has been concluded that more voltage can be scavenged from the nonprismatic beams than the prismatic beam. Moreover, the higher peak of voltage can be attained in Case (C) than Case (B) and (A).

### *3.7 Nonlinear output power responses*

The output power responses from the piezolaminated cantilever beam have been presented in Figs. 11(a)-(d) for $c_b$ =0.2, 0.3 and $c_h$ = 0.2, 0.3 with the geometric nonlinear effects. The magnitude of external excitation has been calculated using the maximum principal stress theory of the beam. Based on this the output power responses have been found out. The external load resistance has been kept constant, i.e., 1 KΩ. From the Figs. 11(a)-(d) it has been observed that the amplitude of output power in Case (C) is more than the Case (B) and (A) in all cases of taper values taken arbitrarily.

### *3.8 Optimal power harvesting by using real coded GA*

To obtain the best set of design parameters as well as

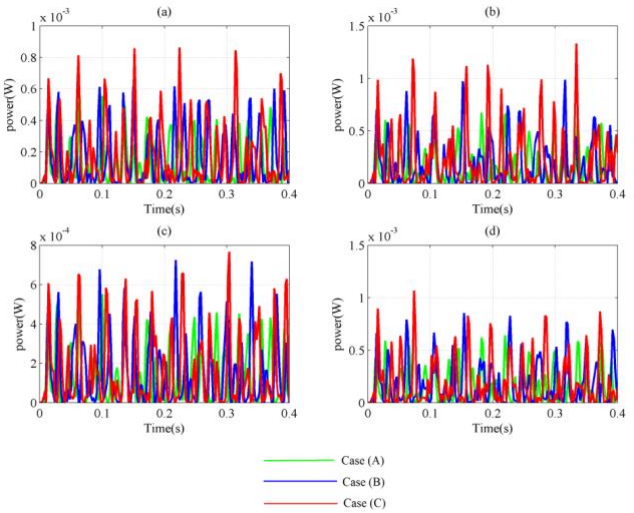


Fig. 11 Nonlinear output power response of Case (A), (B) and (C) for (a) $c_b = 0.2$, $c_h = 0.2$(b) $c_b = 0.2$, $c_h = 0.3$(c) $c_b = 0.3$, $c_h = 0.2$(d) $c_b = 0.3$, $c_h = 0.3$

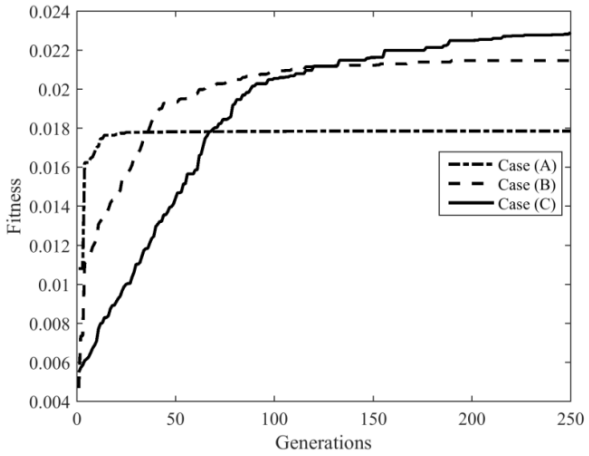


Fig. 12 Comparison of fitness values of Case (A), (B) and (C)

Table 3 Optimal parameters for Case (A),(B) and (C).

| Any arbitrary values of design variables (Trial and Error Method ) | | | | | |
|---|---|---|---|---|---|
| Cases | $c_b$ | $c_h$ | $t_p$(mm) | R(Ω) | Power(W) |
| A | 0.448 | 0.1129 | 0.192 | 8777.3 | 0.0024 |
| B | 0.448 | 0.1129 | 0.192 | 8777.3 | 0.0033 |
| C | 0.448 | 0.1129 | 0.192 | 8777.3 | 0.0042 |
| GA based optimised design variables | | | | | |
| Cases | $c_b$ | $c_h$ | $t_p$ | R | Power(W) |
| A | 0.799 | 0.684 | 0.400 | 9999.56 | 0.0178 |
| B | 0.741 | 0.255 | 0.399 | 9843.67 | 0.0214 |
| C | 0.644 | 0.099 | 0.398 | 9304.47 | 0.0223 |

fitness value using real coded GA, a MATLAB code has been developed. Fig. 12 compares fitness values with generation variation of Case (A), (B) and (C). The best fitnesses for above three cases have been obtained by taking one hundred population with five runs. The obtained

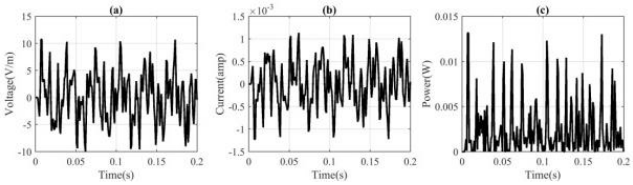


Fig. 13 Optimal responses of (a) voltage (b) current and (c) output power of Case (C)

optimal parameters along with the fitness values are presented in Table 3. Further a comparison of output powers has been made between the trial and error method and the developed real coded GA method which is also listed in Table 3. It is perceived from Table 3 that, more power can be obtained using the developed real coded GA method than trial and error method.

Various responses (such as voltage, current and output power) have also been determined based on an optimal set of parameters of Case (C) represented in Figs. 13(a), (b) and (c).

## 4. Conclusions

The present work focusses on the FE based modelling and analysis of piezolaminated cantilever beam to study the effects of geometric nonlinearity and cross sectional profiles on vibration energy harvesting. A real coded GA-based constrained optimization scheme has also been formulated for the harvesting of optimal output power in the allowable ranges of stresses and voltage of beam and PZT materials. From the study, it is observed that an enhancement of output power can be extracted from the system with an increase in height taper compared to the breadth taper. Furthermore, in Case (C) the output power is more compared to the Cases (A) and (B) for a given breadth and height taper. The geometric nonlinear effects on the output responses (such as voltage and power) have also been discussed to ensure the feasibility of the system in real world problem. Eventually from the proposed GA based constrained optimization scheme, it is perceived that more output power can be obtained compared to an arbitarily selection of design variables by trial and error method.

## References

Abdelkefi, A. (2016), "Aeroelastic energy harvesting: A review", *Int. J. Eng. Sci.*, **100**, 112-135.

Abdelkefi, A. and Barsallo, N. (2016), "Nonlinear analysis and power improvement of broadband low-frequency piezomagnetoelastic energy harvesters", *Nonlin. Dyn.*, **83**(1-2), 41-56.

Abdelkefi, A., Hajj, M. and Nayfeh, A. (2013), "Piezoelectric energy harvesting from transverse galloping of bluff bodies", *Smart Mater. Struct.*, **22**(1), 015014.

Abdelkefi, A., Nayfeh, A. and Hajj, M. (2012), "Effects of nonlinear piezoelectric coupling on energy harvesters under direct excitation", *Nonliear Dynam.*, **67**(2), 1221-1232.

Arora, R., Tulshyan, R. and Deb, K. (2010), "Parallelization of binary and real-coded genetic algorithms on GPU using

CUDA", *Evolutionary Computation (CEC), 2010 IEEE Congress*, 1-8.

Ayed, S.B., Abdelkefi, A., Najar, F. and Hajj, M.R. (2013), "Design and performance of variable-shaped piezoelectric energy harvesters", *J. Intel. Mater. Syst. Struct.*, **25**(2), 174-186.

Bathe, K.-J. (2006), *Finite Element Procedures*, Klaus-Jurgen Bathe.

Benasciutti, D., Moro, L., Zelenika, S. and Brusa, E. (2010), "Vibration energy scavenging via piezoelectric bimorphs of optimized shapes", *Microsyst. Technol.*, **16**(5), 657-668.

Bibo, A., Abdelkefi, A. and Daqaq, M.F. (2015), "Modeling and characterization of a piezoelectric energy harvester under Combined Aerodynamic and Base Excitations", *J. Vib. Acoust.*, **137**(3), 031017.

Bichiou, Y., Abdelkefi, A. and Hajj, M.R. (2016), "Nonlinear aeroelastic characterization of wind turbine blades", *J. Vib. Control*, **22**(3), 621-631.

Biswal, A.R., Roy, T. and Behera, R.K. (2015), "Genetic algorithm-and finite element-based design and analysis of nonprismatic piezolaminated beam for optimal vibration energy harvesting", *Proceedings of the Institution of Mechanical Engineers, Part C: Journal of Mechanical Engineering Science*, 0954406215595253.

Bruch Jr, J., Sloss, J., Adali, S. and Sadek, I. (2000), "Optimal piezo-actuator locations/lengths and applied voltage for shape control of beams", *Smart Mater. Struct.*, **9**(2), 205.

Chuang, Y.C., Chen, C.T. and Hwang, C. (2016), "A simple and efficient real-coded genetic algorithm for constrained optimization", *Appl. Soft Comput.*, **38**, 87-105.

Dai, H., Abdelkefi, A. and Wang, L. (2014), "Piezoelectric energy harvesting from concurrent vortex-induced vibrations and base excitations", *Nonlinear Dynam.*, **77**(3), 967-981.

Dietl, J.M. and Garcia, E. (2010), "Beam shape optimization for power harvesting", *J. Intel. Mater. Syst. Struct*., **21**(6), 633-646.

Erturk, A. and Inman, D.J. (2009), "An experimentally validated bimorph cantilever model for piezoelectric energy harvesting from base excitations", *Smart Mater. Struct*., **18**(2), 025009.

Flynn, A.M. and Sanders, S.R. (2002), "Fundamental limits on energy transfer and circuit considerations for piezoelectric transformers", *Pow. Electron., IEEE Trans.*, **17**(1), 8-14.

Hong, E., Trolier-McKinstry, S., Smith, R., Krishnaswamy, S.V. and Freidhoff, C.B. (2006), "Vibration of micromachined circular piezoelectric diaphragms", *Ultrasonics, Ferroelectrics, and Frequency Control, IEEE Trans.*, **53**(4), 697-706.

Hwang, W. S. and Park, H.C. (1993), "Finite element modeling of piezoelectric sensors and actuators", *AIAA J.*, **31**(5), 930-937.

Javed, U., Abdelkefi, A. and Akhtar, I. (2016), "An improved stability characterization for aeroelastic energy harvesting applications", *Commun. Nonlin. Sci. Numer. Simulat*., **36**, 252-265.

Mehraeen, S., Jagannathan, S. and Corzine, K. (2010), "Energy harvesting from vibration with alternate scavenging circuitry and tapered cantilever beam", *Indust. Electron., IEEE Trans.*, **57**(3), 820-830.

Moheimani, S.R. and Fleming, A.J. (2006), "Fundamentals of Piezoelectricity", *Piezoelectric Transducers for Vibration Control and Damping*, 9-35.

Mukherjee, A. and Chaudhuri, A.S. (2005), "Nonlinear dynamic response of piezolaminated smart beams", *Comput. Struct.*, **83**(15), 1298-1304.

Mukherjee, A. and Chaudhuri, A.S. (2002), "Piezolaminated beams with large deformations", *Int. J. Solid. Struct.*, **39**(17), 4567-4582.

Reddy, J.N. (2014), *An Introduction to Nonlinear Finite Element Analysis: with applications to heat transfer, fluid mechanics, and solid mechanics*, OUP Oxford.

Rosa, M. and De Marqui Junior, C. (2014), "Modeling and analysis of a piezoelectric energy harvester with varying cross-sectional area", *Shock Vib.*, **2014**, 1-9.

Roundy, S., Leland, E.S., Baker, J., Carleton, E., Reilly, E., Lai, E., Otis, B., Rabaey, J.M., Wright, P.K. and Sundararajan, V. (2005), "Improving power output for vibration-based energy scavengers", *Pervasive Comput., IEEE*, **4**(1), 28-36.

Roy, T. and Chakraborty, D. (2008), "GA-LQR based optimal vibration control of smart FRP composite structures with bonded PZT patches", *J. Reinforced Plast. Compos.*, **28**(11), 1383-1404.

Roy, T. and Chakraborty, D. (2009a), "Genetic algorithm based optimal control of smart composite shell structures under mechanical loading and thermal gradient", *Smart Mater. Struct.*, **18**(11), 115006.

Roy, T. and Chakraborty, D. (2009b), "Optimal vibration control of smart fiber reinforced composite shell structures using improved genetic algorithm", *J. Sound Vib*., **319**(1), 15-40.

Xue, H., Hu, Y. and Wang, Q.-M. (2008), "Broadband piezoelectric energy harvesting devices using multiple bimorphs with different operating frequencies", *Ultrasonics, Ferroelectrics, and Frequency Control, IEEE Trans*., **55**(9), 2104-2108.

*BS*